

We are IntechOpen, the world's leading publisher of Open Access books Built by scientists, for scientists

6,900

Open access books available

186,000

International authors and editors

200M

Downloads

Our authors are among the

154

Countries delivered to

TOP 1%

most cited scientists

12.2%

Contributors from top 500 universities



WEB OF SCIENCE™

Selection of our books indexed in the Book Citation Index
in Web of Science™ Core Collection (BKCI)

Interested in publishing with us?
Contact book.department@intechopen.com

Numbers displayed above are based on latest data collected.
For more information visit www.intechopen.com



Vision Based Robotic Navigation: Application to Orthopedic Surgery

P. Gamage¹, S. Q. Xie¹, P. Delmas¹ and W. L. Xu²
¹The University of Auckland, ²Massey University
New Zealand

1. Introduction

Vision guided medical technologies are currently emerging that will influence the way in which orthopedic procedures are diagnosed, planned, simulated, and performed. Medical robotics is one such field that has benefited through the recent advances in the fields of medical imaging and computer vision (Miyamoto, Sugiura et al. 2003).

The orthopedic specialty presents several opportunities to the application of vision guided robotic technology. Radiographic imaging technologies such as c-arm fluoroscopy, X-ray and CT (Computed Tomography) can be used as medical imaging modalities for bony anatomy. The latter is of considerable interest as it enables the building of 3D bone models pre-operatively which permits pose estimation during operative procedures. Moreover, unlike soft tissue, the procedures that involve the manipulation of bones are able to withstand an applied force from tools (robotics) without significant deformation. This has led to the development of orthopedic robotic technologies including several for femur fracture realignment (Joskowicz L, Milgrom C et al. 1998; Graham and Xie 2007; Westphal R, Winkelbach S et al. 2007).

Our work focuses on femur fracture orthopedics with an emphasis on a procedure for fracture reduction called closed intramedullary nailing. The procedure initially requires the alignment of the proximal and distal segments of the bone followed by the insertion of a nail into the medullary cavity of the long bone, typically inserted minimally invasively through the proximal part of the femur. Finally lateral locking screws are placed to hold the nail in place. Intramedullary nailing is performed for cases of femur shaft fractures which are commonly caused by high-energy injury mechanisms (e.g. traffic accidents or heavy falls). Statistics gathered by (Westphal, Winkelbach et al. 2007) indicate an approximate femur fracture incidence rate of 37 per 100,000 persons per year, and thus it is a frequently encountered injury. In 2004, 3200 patients with fractures of the thigh bone have been counted in New Zealand (Cure-Research 2004). These figures include fractures in the proximal (hip side) femur as well as the shaft (the middle, diaphyseal) region.

Intra-operative fluoroscopy is the imaging modality utilized for visualizing underlying bone and surgical tool positions in femur fracture orthopedic procedures. Fluoroscopic image guidance of robotic systems can be divided into two categories: 1) open loop calibrated guidance 2) closed loop un-calibrated guidance. Open loop calibrated guidance methods

compute the robot's spatial localization with respect to the camera coordinate system by imaging a target with known geometry. The desired robot pose is then specified, either automatically or manually, in the camera coordinate system and the robot is aligned accordingly. Since the internal camera parameters are required for robot pose estimation, the c-arm must be calibrated. Closed loop un-calibrated methods guide the robot to the desired pose based solely on the acquired images. The desired target pose is specified, either automatically or manually, in the image coordinate system. The robot pose is then updated continuously according to the images, until the desired pose is attained.

We have opted for closed loop guidance due to the reduction in pre-operative imaging that is required. The main difference in requirement between the open and closed loop systems is in the definition of the robot target pose. Closed loop methodologies require the 3D volumetric model to be registered to the intra-operative situation using a 2D-3D registration technique. This defines the robot target pose intra-operatively. The focus of the chapter is placed on new methods and technologies for performing the aforementioned 2D-3D registration. The chapter will discuss the developed algorithms to recognize the object to be manipulated by matching image features to a geometrical model of the object and computing its position and orientation (pose) relative to the robot coordinate system. This absolute pose and cartesian-space information is used to move the robot to the desired pose. Apart from fracture reduction, hip and knee arthroplasties and several spinal procedures are currently seen as potential areas of orthopedics benefited by intra-operative 3D pose estimation, through a 2D-3D registration process. Literature work that conduct tracking of fractured bone segments through intra-operative 2D-3D registration can be seen in (Joskowicz L, Milgrom C et al. 1998; Westphal R, Winkelbach S et al. 2007; Gamage, Xie et al. 2008). Intra-operative pose estimation techniques could further be used during spinal orthopedic procedures such as reinforcement of falling vertebra and pedicle screw placement (Penny 1999; Zollei 2001; Tomaževic, Likar et al. 2003). Furthermore, in hip arthroplasty, the positioning and implanting of the acetabular cup into the pelvic bone can also be aided through intra-operative pose estimation (LaRose, Cassenti et al. 2000; Hüfner, Meller et al. 2005). Several other (non orthopedic) areas for the use of intra-operative pose-estimation has been identified as radiotherapy (Bollet, Mcnair et al. 2003) and endovascular treatments (Zollei 2001; Tomaževic 2002).

The pose estimation work conducted by the authors is motivated by a recent study conducted on femur fracture reduction, which demonstrated a shift towards 3D visualization modalities. It confirmed that computer-aided systems significantly improve the accuracy of orthopedic procedures by augmenting the current 2D image guidance with interactive display of 3D bone models (Joskowicz L, Milgrom C et al. 1998). Research indicates that the positioning errors and complications that are seen in 18% of femur fracture cases and the misalignments created would be reduced with the introduction of an interactive display of 3D bone models into the fracture reduction process (Joskowicz L, Milgrom C et al. 1998).

This chapter is divided into three main sections. The first section documents the current state-of-the-art research in pose estimation associated with orthopedic IGS systems. Section two presents the proposed methodology in full detail. Section three provides the results of the tests conducted.

2. Literature Review

Several methodologies that tackle the problem of intra-operative registration of bony anatomy in orthopedic surgery appear in literature. The schemes developed by (Joskowicz L, Milgrom C et al. 1998; Westphal R, Winkelbach S et al. 2007) track the bone fragments in real-time by means of an optical tracking system using a set of infrared markers. Thus to track the position of the distal and proximal bone fragments, the surgeon implants fiducial markers into the bone segments. These physical tracking methodologies are accurate. However the implanting of the optical trackers on the bone is an arduous task for the surgeon/technician who already deals with a narrow field of view with the present system. Another drawback of such systems is the guidance inaccuracies caused due to movement, deformation and changes in anatomy since the time of initial imaging. Furthermore optical tracking requires a direct line of sight between the LED assembly on the patient and the external sensor assembly. This is a cumbersome requirement in a crowded operating theatre. Moreover, this would also introduce new training and process requirements that would limit the performance of the surgery. These difficulties hinder the widespread introduction of fiducial marker based intra-operative tracking into orthopedic procedures.

Several other studies have performed image based registration between intra-operative x-ray/fluoroscopic images and the pre-operative 3D CT data of the anatomy of interest. These methodologies can be grouped as feature based registration techniques (Besl and McKay. 1992; Taylor, Mittelstadt et al. 1994; Lavalley, Szeliski et al. 1995; Livyatan, Yaniv et al. 2003; Tomaževic, Likar et al. 2003) or as intensity based registration techniques (Penney, Batchelor et al. 2001; Zollei, Grimson et al. 2001; Rohlfing and Maurer 2002).

Feature based approaches rely on the presence and identification of natural landmarks in the input datasets in order to determine the best alignment. Feature based techniques can be again subdivided into either point based or surface based techniques depending on the type of 3D data utilized. Feature point based methodologies identify corresponding landmark points on the 2D image and 3D volume (Taylor, Mittelstadt et al. 1994). These key feature points can be defined manually or through some automatic feature identification process. In this scenario the 2D-3D registration is concerned with minimizing the distance between the two point sets after the 3D landmark points are projected onto the 2D plane. Surface based (Besl and McKay. 1992; Lavalley, Szeliski et al. 1995; Livyatan, Yaniv et al. 2003; Tomaževic, Likar et al. 2003) feature registration approaches utilize the outer surfaces of an object of interest (extracted from a 3D model), and contours that outline the object on one or more 2D images. Registration is concerned with finding the object pose that minimizes the distance between surface and the contour. One way to achieve this minimum is by extending 3D projection lines from points on the contour in the 2D image to a point representing the X-ray source. Then the distance to be minimized can be represented as the Euclidean distance between a projection line and the nearest point on the 3D surface (Lavalley, Szeliski et al. 1995). Another methodology is to project 3D surface points onto the 2D plane and then attempt to minimize the distance between the contour of the projected image and the initial 2D contour. The work done by (Lavalley, Szeliski et al. 1995; Livyatan, Yaniv et al. 2003; Tomaževic, Likar et al. 2003) has presented another methodology where projections of the volumetric data gradients are computed and compared with X-ray image gradients. The volumetric data pose is adjusted to minimize this gradient difference.

Intensity based measures operate on the pixel or voxel intensities directly. They calculate various statistics using the raw intensity values of the inputs which are then compared in

the images to be aligned (Penney, Weese et al. 1998). The matching can be restricted to regions of interest (ROIs) in the image, such as regions around bone surfaces in CT and fluoroscopic images, or the entire acquired image. Intensity based registration consists, generating digitally reconstructed radiographs (DRRs) for each pose, measuring the pose difference by comparing the DRRs with the fluoroscopic images through a similarity measure, and finally computing a pose that minimizes that difference. The calculation of a DRR by numerical summation of CT image intensities along projection rays involves high computation cost and is thus time consuming. Number of methods have been proposed that simplify and consequently speeds up the calculation of DRRs, without losing information that is needed for registration (LaRose, Bayouth et al. 2000). The similarity measure performed between the DRR and the acquired radiograph is important as it dictates the success of the optimization process. Work has been done by Penny et al. (Penney, Weese et al. 1998) where several similarity measures for registration of 3D CT and 2D X-ray images were tested providing some insight to the possible choice of an adequate similarity measure. Though the number of points to be registered is much greater than in the case of the feature-based methods, the key characteristic of intensity-based registration is that it does not require segmentation and feature extraction, thus reducing the influence of outliers and increasing robustness.

Due to the timeliness exhibited by feature based registration methodologies the intra-operative pose estimation framework proposed in this chapter has made use of this technique. Although related registration methodologies have been developed in the past, there remain significant challenges as these methodologies have not yet been introduced into fractured bone segment pose estimation. The anatomy based intra-operative pose estimation framework proposed in this chapter is motivated by these limitations.

3. Methods

Fig. 1 illustrates the proposed framework and conveys how the 2D-3D registration algorithm is used intra-operatively along with the pre-operatively reconstructed 3D fractured bone model. The 2D-3D registration framework can be split into two distinct phases: 1) Frontal and lateral pose estimation 2) Axial pose estimation. Since the registration is performed through images acquired from the frontal and lateral viewpoints, registration in these planes will be performed highly accurately through the first phase of the 2D-3D registration process. The axial alignment, which is critical as it has a high impact on functional biomechanics of the leg, will be conducted in the second phase. The intra-operative 2D-3D registration framework discussed is independent of how the patient-specific 3D data is acquired. The proceeding sections will discuss the required processing of the fluoroscopic images to extract the features of interest, CT dataset segmentation for patient-specific model creation, followed by the 2D-3D registration algorithm.

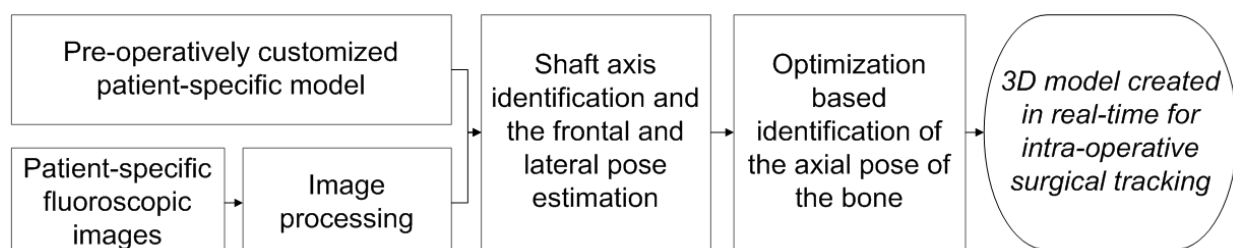


Fig. 1. The main process steps of the proposed framework.

3.1 Acquisition Geometry and Calibration of Fluoroscopic Images

In this chapter the fluoroscopic image acquisition is described through a pinhole camera model (Tsai 1987), that represents mapping from a 3D scene onto a 2D image (Fig. 2).

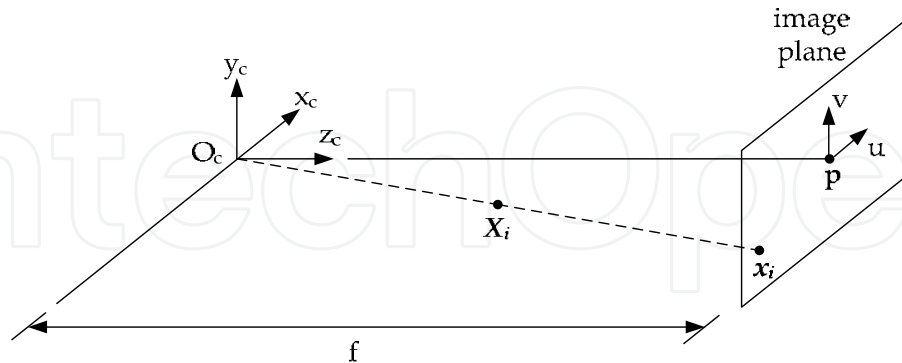


Fig. 2. Pinhole camera model showing camera centre (O_c), principal point (p), focal length (f), 3D point (X) and its image projection (x).

The X-ray center of projection is defined as O_c and the imaging plane is located at $z_c =$ focal length (f). The ray from the center of projection to the image plane is called the principal axis, and the principal point (p) is the point at which the light that passes through the image is perpendicular to the imaging plane. The pinhole camera model dictates that 3D object points X_i map onto the imaging plane through the intersection of rays that originate from the centre of projection and pass through X_i . Simple geometry shows that the image coordinates (u, v) are related to the object coordinates (x_o, y_o, z_o) , of point X_i , through Equation (1).

$$u_i = \frac{f}{z_o} x_o \quad \text{and} \quad v_i = \frac{f}{z_o} y_o \quad (1)$$

The relationship between the coordinates of a 2D image pixel, and its corresponding 3D object point can be expressed through Equation (2) below.

$$x = MX \quad \text{where} \quad M = K[R | t] \quad (2)$$

Here the 3x4 projection matrix M , relates any 3D point $X = (x_o, y_o, z_o, 1)^T$ to its corresponding projection $x = (u, v, 1)^T$ in the acquired image. The intrinsic projection parameters of the X-ray tube (focal length and principal point coordinates), are represented through K , and the extrinsic parameters (rotation and translation of the acquisition system in a world coordinate system) through $[R | t]$. The intrinsic projection parameter matrix can be defined through Equation (3). Here (u_o, v_o) denote the coordinates of the principal point. The pixel sizes along the u and v axes is denoted by pix_u and pix_v respectively.

$$K = \begin{bmatrix} \frac{f}{pix_u} & 0 & u_o & 0 \\ 0 & \frac{f}{pix_v} & v_o & 0 \\ 0 & 0 & 1 & 0 \end{bmatrix} \quad (3)$$

The camera calibration methodology is not an integral part of this chapter. The intrinsic camera calibration method simply relies on the technique described in (Tsai 1987) where a set of coplanar points visible on the image, are used to compute the camera parameters. We utilized a radio-opaque board with spherical metal markers applied to it on both sides. The respective positions of the markers on the fluoroscopic images are identified through segmentation. In order to obtain the intrinsic parameters, a set of views of the calibration board at different poses is used. First the parameters are approximated by a closed-form solution which disregards lens distortion. Then the reprojection error is minimized using gradient descent yielding the final values for the intrinsic parameters.

The extrinsic parameters relating to the rotation R and translation T of the acquisition system are computed for different c-arm orientations. The c-arm orientation is described by two anatomical angles, cranio-caudal(a) and right/left anterior (β) and a translational adjustment between the source and the imaging object (Source to Image Distance, or SID). The SID and the a/β angles are measured in real time by sensors (Fig. 3). The extrinsic parameters of the c-arm are modeled as a function of a and β angles (Equation 4). Here, R_o is the rotational matrix describing the initial ($a=0$ and $\beta=0$) local camera frame with respect to the global coordinate frame. T_o is the initial ($a=0$ and $\beta=0$) translation of the center of projection in global reference frame coordinates. R_{α_i} is the rotational transformation due to rotation of α_i about the resulting alpha axis. R_{β_i} is the rotational transformation due to rotation of β_i about the constant beta axis. It is assumed that both axes are orthogonal and intersect.

$$\begin{aligned} R &= R_o^T R_{\beta_2} R_{\alpha_2} R_{\beta_1}^T R_{\alpha_1}^T \\ T &= R_o^T (R_{\beta_2} R_{\alpha_2} - R_{\beta_1} R_{\alpha_1}) T_o \end{aligned} \quad (4)$$

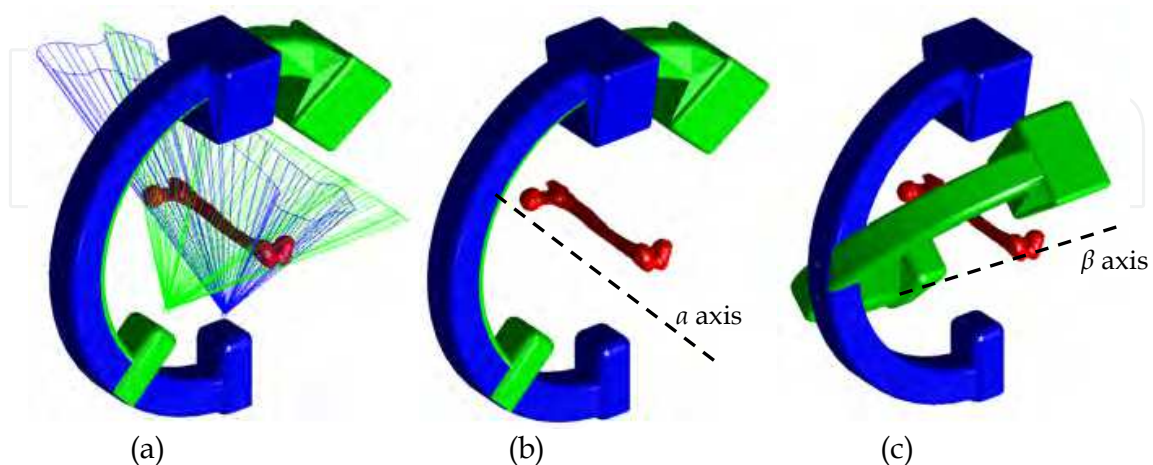


Fig. 3. The c-arm in numerous orientations. From left to right: (a) Illustration of the effect of the pinhole camera model applied to the c-arm setup ; (b) Example of a 45 degree rotation about the a axis; (c) Example of a 45 degree rotation about the β axis.

3.2 Fluoroscopic Image Processing

Image processing is performed on the fluoroscopic images to extract the necessary feature information for the 2D-3D registration process. The processing performed can be separated into two stages: segmentation (edge extraction) and key morphological feature extraction (femur shafts).

The main objective of the edge extraction technique is to identify object boundaries with sufficient continuity to be successfully employed in the proceeding pose estimation. Many of the classic first (Roberts, Prewitt, Sobel) and second (LOG) derivative based edge segmentation methodologies extract isolated edge pixels and do not provide continuous edge contours. The proposed edge extraction technique attempts to link sets of potential edge pixels to create continuous boundaries. It employs two tactics to achieve this: thresholding with hysteresis and edge relaxation.

Firstly, adaptive (local) hysteresis based thresholding is performed on the gradient image where the two threshold values are set to be the 50th and 75th percentile of gradient magnitude values in the local window. Adaptive thresholding adjusts the threshold level according to the intensity statistics of a local region. This technique is employed typically with X-ray/fluoroscopic images to counter the illumination gradients present on the radiographs.

Secondly, edge relaxation is performed through a region growing exercise. This region growing is conducted on the intermediate pixels (pixels that fall between the 50th and 75th percentile of gradient magnitude values) to ensure sufficient continuity of the edge contour. Edge relaxation involves the recursive re-labeling of intermediate pixels with one or more neighboring edge pixels, utilizing an eight neighboring connectivity scheme. In-order to be reclassified as a foreground edge pixel the difference of the magnitude and orientation of the intervening pixel with the surrounding edge pixels will be checked and has to be within a user specified tolerance level. Following the edge relaxation a small component elimination morphological operation is performed to remove all connected pixel components with too few pixels. This is a noise elimination step that will remove any misidentified edge contour pixels.

Following the edge extraction, further image processing is conducted to identify the femur edges that form the outer diameter of the shaft. A classical Hough transform is used to isolate these feature lines within the segmented fluoroscopic image. The classical Hough transform requires that the desired features be specified in some parametric form, and hence is ideal to be used for the detection of regular shapes such as lines. The main advantage of the Hough transform technique is that it is tolerant of gaps in feature boundary descriptions and is thus unaffected by slight image occlusions (Beutel, Kundel et al. 2000).

Once potential lines have been identified through the Hough transform they will be paired and classified as an outer edge or noise (Fig. 4). This classification is performed by utilizing data gathered by (Noble, Alexander et al. 1988) on the mean and variance of femur shaft cross sectional anthropometry. Thus line pairs that fall within a certain range (mean \pm standard deviation) of the anthropometric measurements will be classified as a pair representing the outer diameter of the shaft. The edge contour image that will result following the segmentation and the extracted feature lines will provide the required input to the 2D-3D registration process as will be discussed in the proceeding section.

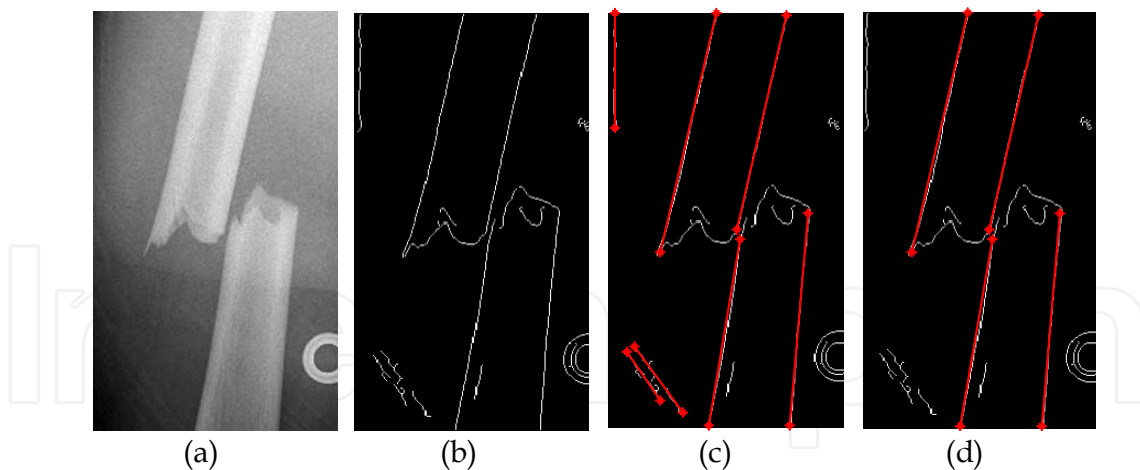


Fig. 4. An example of the segmentation and feature extraction operations that are performed on the radiographic images. From left to right: (a) Original image; (b) Segmented Image: Edge Extraction; (c) Feature lines identified through the Hough transform; (d) Paired shaft lines.

3.3 Extraction of Anatomical Surface Model

The patient-specific 3D anatomical bony structures required for the intra-operative registration are pre-operatively extracted from CT data. Bony anatomies appear as high intensity regions in the CT slice images. Reconstruction of 3D models from CT volumes consists of a two-step process. Firstly, an image slice segmentation is required for the extraction of the outer contours of the anatomical structures, and secondly, 3D reconstruction is performed by utilizing a surface triangulation technique such as the marching cubes algorithm (Kim, Kim et al. 2004; Momi, Motyl et al. 2005). Femoral contour extraction is a difficult process due to the variation in the bone intensity and the lack of a distinct joint space. The interior structure of the femur contains trabecular bone with a shell of cortical bone. The image intensity varies between these two bone structure types. Furthermore, weakly defined joint space around the femoral head and the pelvic bone also adds to the complexity of the contour extraction process.

Several techniques that appear in literature were considered to perform the segmentation and contour extraction. Atlas based segmentation techniques merge image segmentation with image registration (Beutel, Kundel et al. 2000). However, fractured bone segmentation is not possible through this technique. Region growing approaches can segment whole skeletal structures, but cannot separate individual bones (Beutel, Kundel et al. 2000). Thus a Level-Set based segmentation technique was developed to provide adequate flexibility to segment fractured bones while ensuring the ability to extract only femoral bone fragments of interest. Level-Set methods have been widely used in the fields of fluid mechanics and material sciences for some time and have recently been applied within the field of machine vision for segmentation problems (Li, Xu et al. 2005).

The principal idea behind level set methods is the definition of a static, evenly spaced mesh in an image or volume space. The values at each point on the mesh relate to the proximity of the mesh point to an evolving curve or surface with the level set of zero defining the location of the curve or surface. Mesh points contained within the evolving surface are given negative values and mesh points outside the surface are given positive values. An evolving speed function for the movement of the curve or surface is defined and mesh values are

updated (from an initial value) using a discrete time finite element update as described in Equation 5. Let the moving interface be $\Gamma(t) t \in [0,1]$ and the level set function as $\phi(x) = \pm d$. Where d is the distance between the point \mathbf{x} and $\Gamma(t)$, and the plus/minus sign is chosen depending on whether the point is outside/ inside the interface.

$$\phi_{t+1} + F|\nabla\phi_t| = 0 \quad (5)$$

In the above equation, F is the speed of the interface point along its normal direction. The moving interface evolves under the effect of F . It expands when F is positive, while it contracts when F is negative. When F is equal to zero, the interface stops and gives the segmentation result. The method implemented is a 3D level set which forms a single unconstrained 2D surface in 3D space. The formulation of the speed function is given in equation below. The speed function F controls the deformation of the interface.

$$F(x,y) = (F_0\nabla\phi_{x,y} + F_c(x',y')\nabla\phi_{x',y'})e^{-F_i(x',y')} \quad (6)$$

In the above equation $F(x,y)$ is the force at mesh point (x,y) and (x',y') is the nearest point on the zero level set to (x,y) . F_0 is the Advection Force term, F_c the Curvature Force term and F_i the Image Force term based on the Gaussian derivative filters.

The image force term F_i is based on a 1D Gaussian derivative filter orientated in the normal direction of the zero level set surface at the point of interest (x_0, y_0) .

This filter is preferable over a simple edge detection such as a Sobel or Canny edge detector as its increased range means that less defined edges may be detected.

Level set methods have a high computational cost as the nearest point on the zero level set must be found for each mesh point. Narrow-band extensions to level set methods lower the computational cost of the algorithms by only updating the mesh in an area local to the zero level set. These methods require the mesh to be reinitialized every few time steps as the zero level set approaches the mesh points that have not been updated. This re-initialization is in itself computationally expensive, however the overall computational cost over time was reduced substantially using this method.

The narrow band update method was used in the implementation with a band range of 5 in plane voxel widths. It is useful to note that mesh values may be used to determine how close to the level set the mesh point is and whether it is inside or outside the level set, based on the sign. A relatively large time step is used in our implementation as smaller time steps do not appear to affect the final result and increase the computational cost. The Advection Force is set to unity.

Following the segmentation, a 3D triangulated surface may be formed from the mesh by iso-surfacing with the value zero using the 'Marching Cubes' algorithm (Kim, Kim et al. 2004; Momi, Motyl et al. 2005). This algorithm is based on examining each 8 adjacent points in the mesh and determining the triangulation required.

3.4 Pose Estimation

The proposed pose estimation framework employs the set of 2D fluoroscopic images and the 3D anatomical surface model, and identifies the transformation of the model so that its projections on the anterior and lateral planes match the acquired fluoroscopic images. This registration can be treated as determining the equivalent affine transformation which includes a set of translational (T_x, T_y, T_z), and rotational (R_x, R_y, R_z) parameters where the x, y and z axes are aligned with the frontal, lateral and axial axes of the bone segment. As illustrated in Fig. 5 the 2D-3D registration between a 2D projection image and 3D model is concerned with determination of the transformation $T_{2D/3D}$ such that the 3D to 2D projection fulfils the conditions defined above. The image to physical space registration (T) can be described as finding the geometrical transformation that determines the position of the imaged anatomy in the world coordinate system.

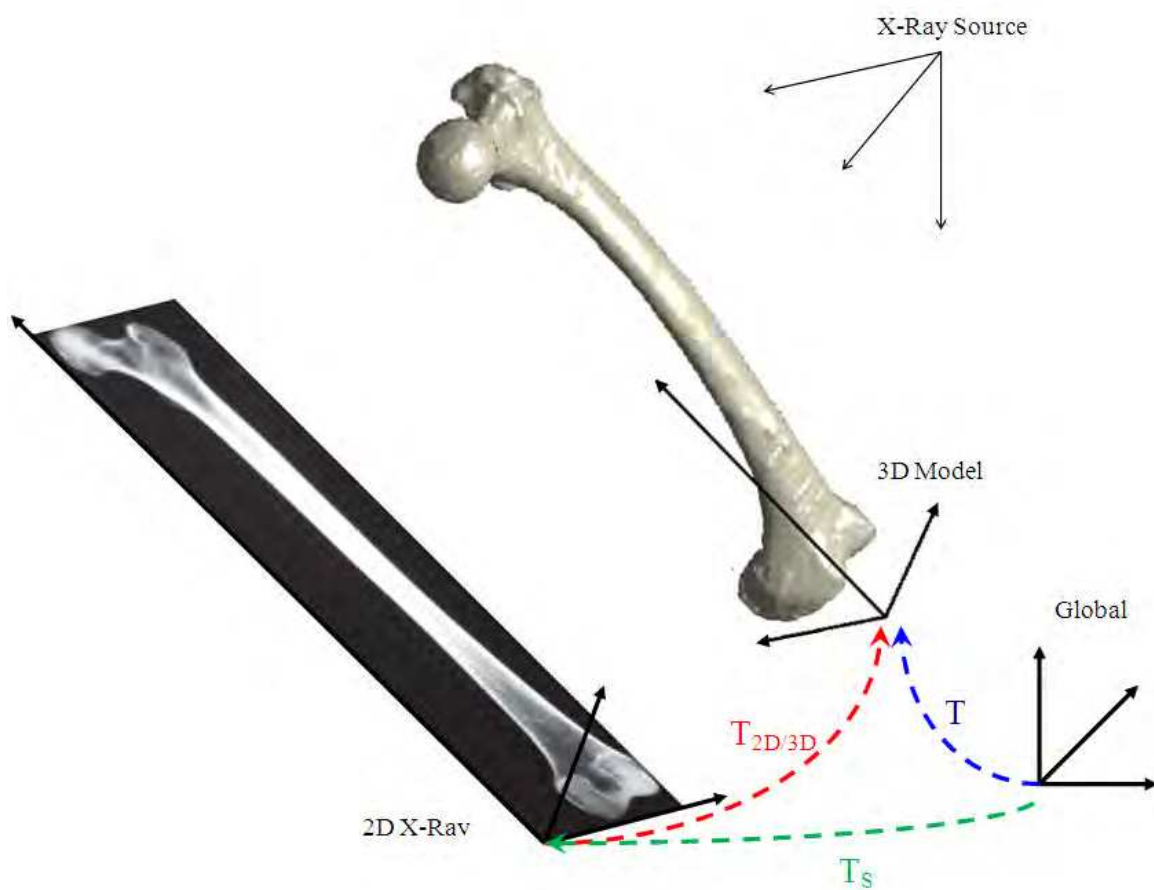


Fig. 5. 2D-3D registration ($T_{2D/3D}$) and 3D image to physical space registration (T). A pin-hole projection model is used here for illustrative purposes.

The frontal and lateral alignment is driven by the outer shaft lines identified through the fluoroscopic image processing. The inputs required for this alignment are the two 2D gradient directional vectors of the shaft in the frontal and lateral planes as well as two arbitrary points that lie anywhere on the mid shaft axis in those planes.

Firstly the mid shaft line is calculated by averaging the start and end points of the outer shaft lines in each plane (from which the required directional vectors and the arbitrary

points are extracted). This mid shaft line is then projected perpendicular to the plane. The intersection of these perpendicular projections from the frontal and lateral planes will form the axis of rotations for a particular segment (Fig. 6). The gradient information of the mid shaft line is utilized to calculate the normal vectors of these projected planes by obtaining the cross product between the direction vectors of the mid shaft lines and the imaging plane normals. These normal vectors, $n_{frontal}$ and $n_{lateral}$ and the arbitrary points identified on the lines ($P_{frontal}$ and $P_{lateral}$) are used in Equation (7) to solve for the vector line equation of the shaft axis of rotation in 3D. This is accomplished by identifying a point that lie on the 3D axis of rotation (P_{axis}) as well as the direction vector of the axis (M_{axis}) as seen in Equation (7).

$$P_{axis} = (pinv(A)) \begin{bmatrix} n_{frontal}^T P_{frontal} \\ n_{lateral}^T P_{lateral} \end{bmatrix}, \quad M_{axis} = Null(A) \quad (7)$$

$$where \quad A = \begin{bmatrix} n_{frontal}^T \\ n_{lateral}^T \end{bmatrix}$$

Once the axis of rotation is identified for the target images, the model axis of rotation can then be aligned with it utilizing Equation (8). Here $^{model}T_{global}$ and $^{target}T_{global}$ are homogeneous transformation matrices which relate the local coordinate frames of the bone segments to a global coordinate frame. The z-axis of these local frames coincide with the axial rotation axis of the bone segments, while their origins are anchored on the corresponding feature points in the model and target bones. The final alignment transformation between the model and the target is then expressed as, $^{model}T_{target}$.

$$^{model}T_{target} = ^{model}T_{global} \left[^{target}T_{global} \right]^{-1} \quad (8)$$

$$^{model}T_{target} = ^{model}T_{global} \quad ^{global}T_{target}$$

It should be noted however that the axial alignment of the coordinate frames with respect to the bones may not be identical in both the model and the target. As a result, even after the application of the transformation obtained in Equation (8), a final adjustment of the axial rotation is still required to complete the pose estimation process. This axial alignment process is discussed in the proceeding section. Fig. 6 illustrates the various notations involved in the axis of rotation identification process. Fig. 7(a)/(b) illustrates the axial alignment process.

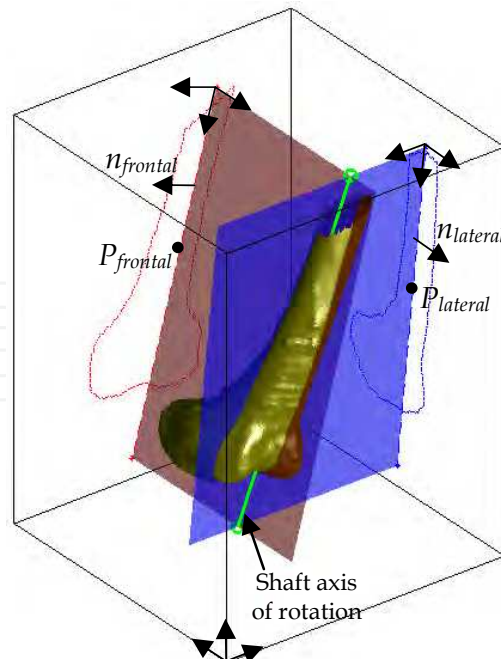


Fig. 6. The notations involved in the axis of rotation identification process for the frontal and lateral alignment.

Following the anterior and lateral pose estimation the axial rotational and translational alignment is conducted through an optimization based framework. The objective functions (similarity measure) proposed for this task is the summation of the Euclidean distance between each surface boundary contour point of the projections from the 3D surface model and the corresponding closest point on the edge contour identified on the fluoroscopic image. Fig. 7(b) illustrates the objective function for variations of angular axial rotations (R_z direction). The objective function posed through the similarity measure that is proposed can be classified as Nonlinear, Continuous, Unconstrained and Deterministic. Arguably the problem can be classified as a constrained optimization problem with constraints imposed on the possible transformations. However, these constraints will not play an essential role in the optimization and will only serve as general safety limitations and hence were excluded from the optimization process. Many algorithms for nonlinear optimization problems seek only a local solution, and do not always identify the global optima. The logical methodology to ensure the global convergence is to ensure that the problem is one of convex programming. For a convex function, global optimality is guaranteed by local optimality. The current objective function shown in Fig. 7(b) has the required convex shape (in the proximity of the optima). The simplex Nelder-Mead method (Lagarias, Reeds et al. 1998) was utilized to solve this multivariable optimization problem. The optimization process is run under two conditions that ensure successful convergence and timeliness. Firstly, a multi-resolution framework is employed that involves first searching for the solution from a highly sub-sampled projected contour and then refining the solution through a series of reductions to the sub-sampling. Secondly a variable step size based implementation is employed where the rotation and transformation steps start with large sizes and iteratively lessens in size as the algorithm nears its optimal solution.

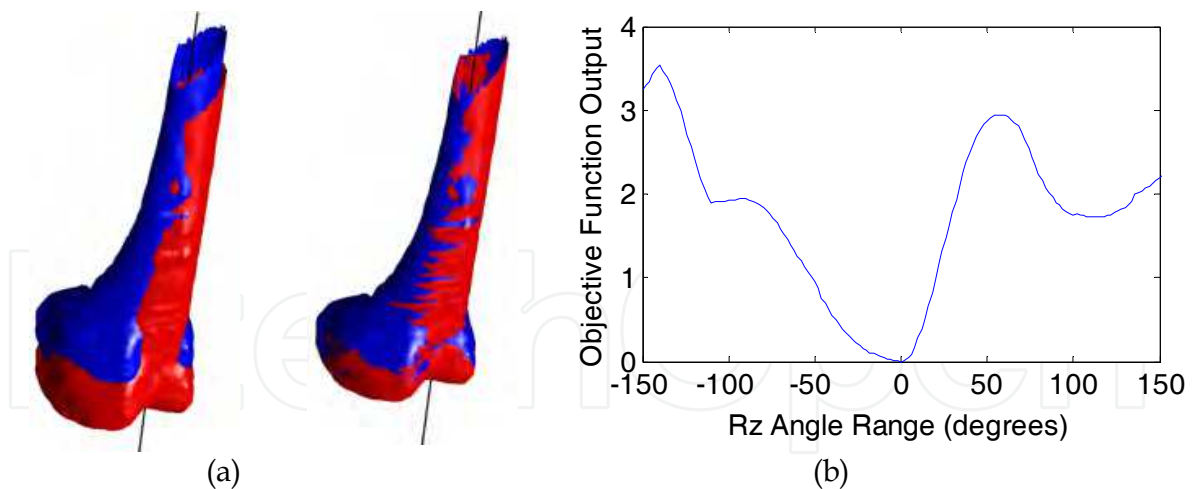


Fig. 7. Illustrations of the pose estimation stages proposed in this chapter. From left to right: (a) The axial alignment process, where the images show the before and after illustrations of aligning the model and target bones axially; (b) The objective function output for variation in the axial (R_z) direction. The registration used anterior and lateral target images acquired at the neutral position of R_z being set to zero.

4. Results

To test the pose estimation capabilities of the 2D-3D registration algorithm and the effectiveness of the proposed similarity measure (objective function) several phantom studies were conducted.

The first study involved a synthetically broken CT data set from which pairs of fluoroscopic images were acquired in the frontal and lateral planes. This acquisition was repeated for a series of poses of the CT data. Through this synthetic CT volume movements the authors were able to obtain highly realistic fluoroscopic images that were analogous to those obtained clinically on human subjects (Fig. 8). These acquired fluoroscopic images were next utilized in the testing phase where the 2D-3D registration was performed with a prebuilt 3D surface model of the fracture region. This 3D model was acquired from the CT data set and was initialized manually. Fig. 8 illustrates a few qualitative results of the tests performed. Moreover, Table 1 indicates the absolute average difference between the actual and identified rotations/translations through the 2D-3D registration process.

Digitally Reconstructed Radiographs (DRRs) simulating the fluoroscopic images were created from the CT dataset utilizing ray-casting. This technique initially constructed rays between points on the imaging plane and the imaging source and then the individual intensity values of the DRR images were computed by summing up the attenuation coefficients associated with each voxel along a particular ray in the CT data.

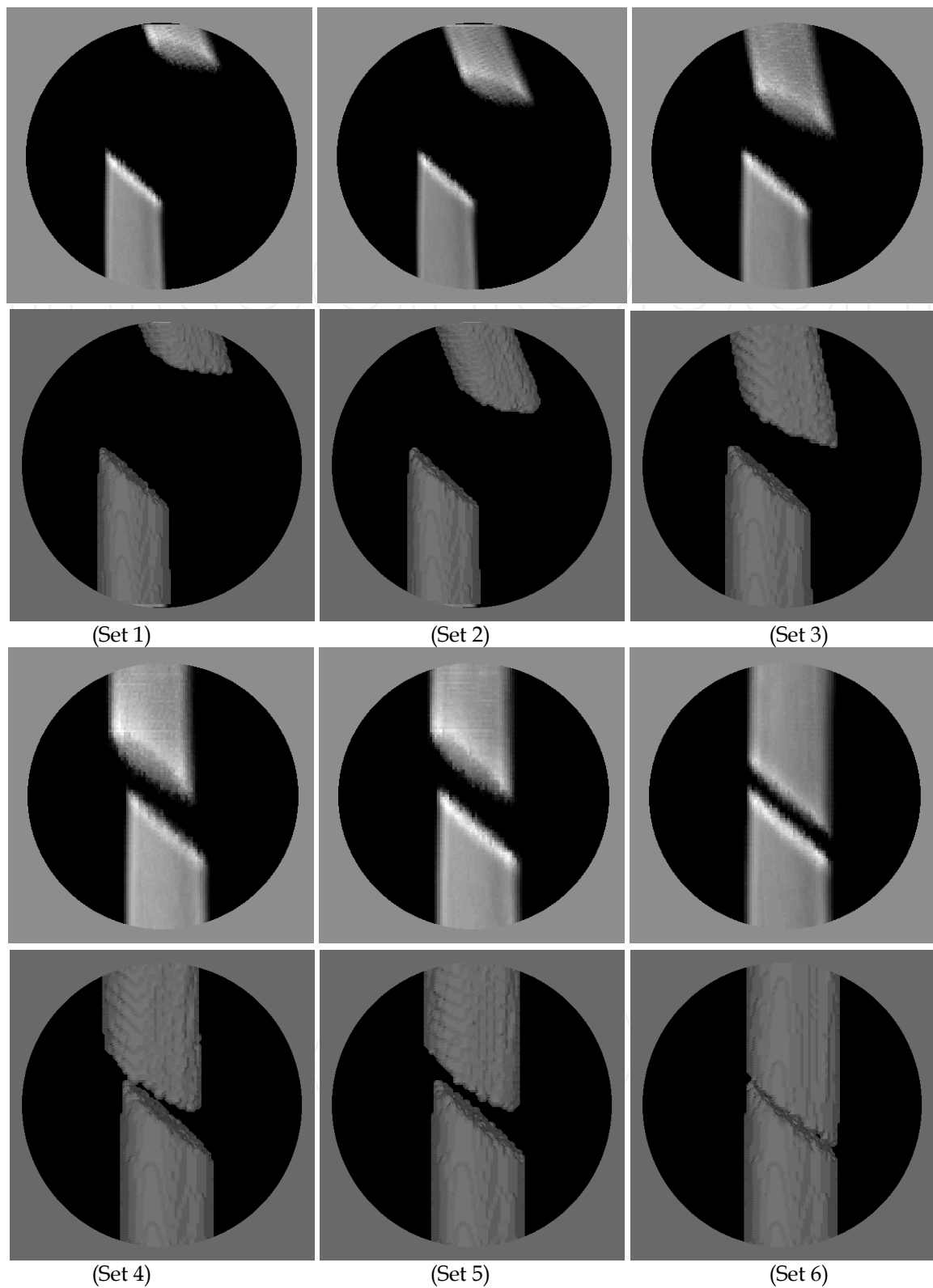


Fig. 8. Qualitative results of the pose estimation performed on the series of phantom fracture reduction fluoroscopic images (Study 1). Each set of paired images represents a pose that was estimated through the 2D-3D Registration algorithm. The top image of each set is the frontal fluoroscopic image generated while the bottom is the registered 3D bone fragments overlaid on the fluoroscopic images.

The results in Table 1 convey that the registration was performed at sub-degree and sub-mm accuracy and with highly robust repeatability. This is in line with the accuracy requirements for image guidance required during present orthopedic femur fracture reduction procedures.

The second study was performed with a distal fragment of an artificially fractured plastic bone (Fig. 9). The fragment was attached to a Stewart platform and moved through a series of rotations in the R_x , R_y and R_z direction. Fluoroscopic imaging was emulated through a USB camera mounted on a rotary arm (similar to a fluoroscopy c-arm). Even though the effects of variation of X-ray absorption in tissues such as muscle, fat, and skin cannot be simulated with this test setup, effort was made to closely match the actual clinical process steps undertaken. The proposed pose estimation technique was applied to this test setup and 20 iterations of the same test were conducted (Fig. 10). The average absolute mean R_x error was 0.567 degrees, R_y error was 0.487 degrees and the R_z error was 0.604 degrees. The standard deviation of errors was 0.098 degrees. The results further convey that the registration can be performed at sub-degree accuracy.

Pose Iteration	Rotational Registration Average Error (Degrees)	Translational Registration Average Error (mm)
1	0.965	1.056
2	0.710	0.981
3	0.862	1.198
4	0.997	0.912
5	1.069	0.896
6	1.159	1.287

Table 1. 2D-3D registration results for Study 1.

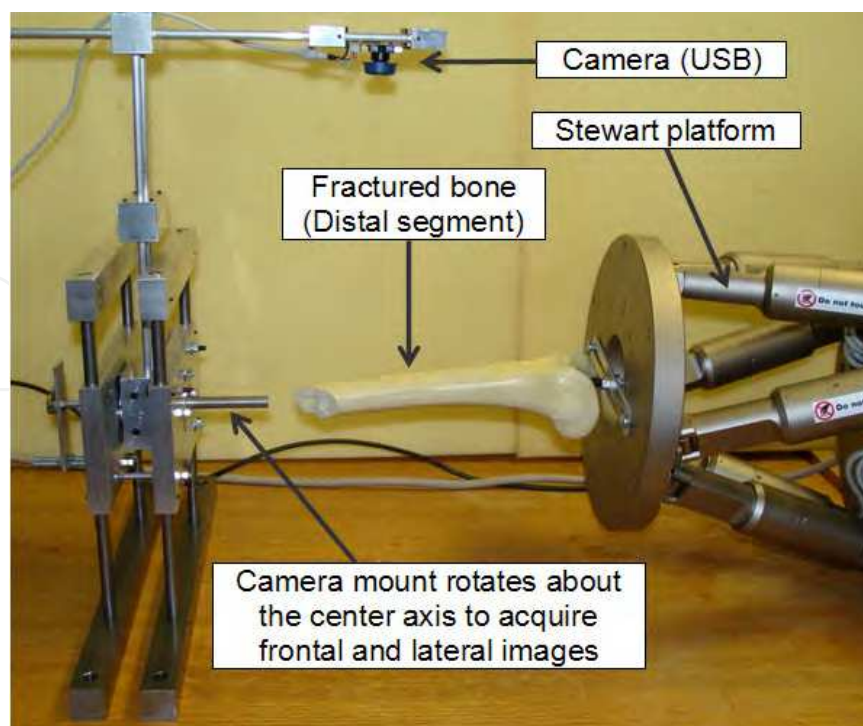


Fig. 9. The test rig setup.

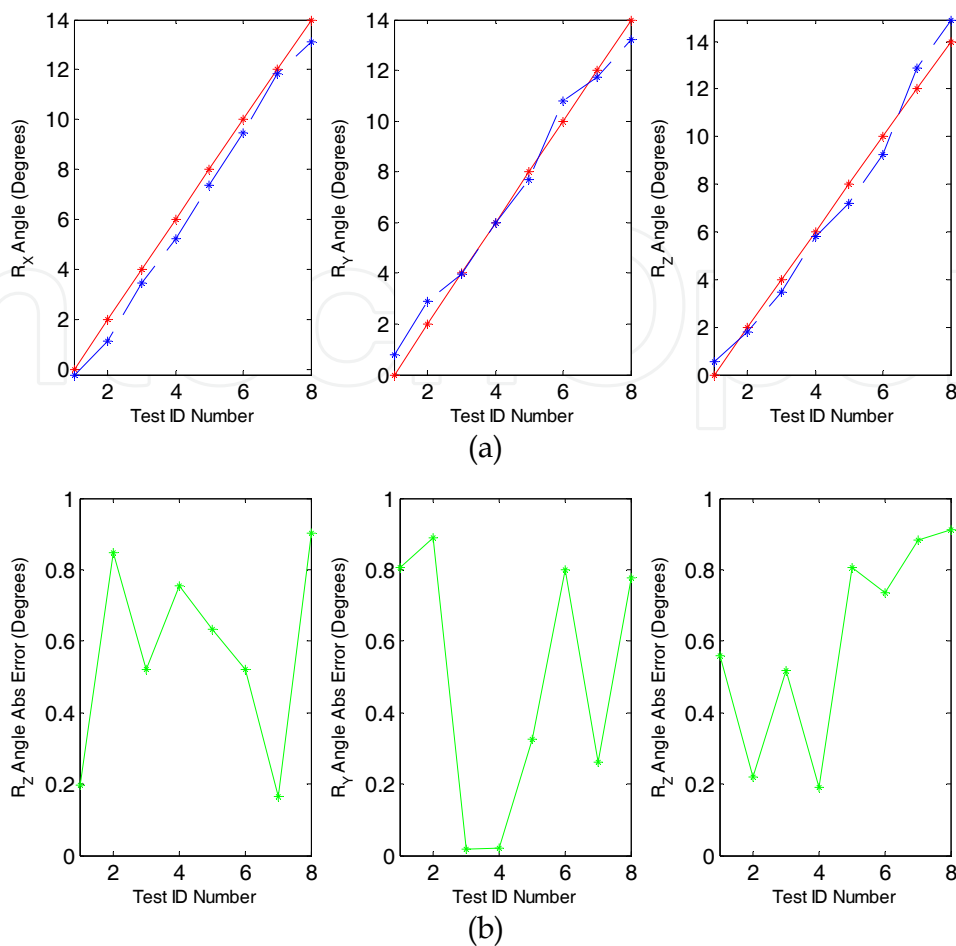


Fig. 10. Results obtained with the Stewart platform tests. From top to bottom: (a) Results obtained in the frontal (R_x) lateral (R_y) and axial (R_z) directions. The red lines indicate the rotation of the Stewart platform, while the blue lines indicate the identified rotation in the R_x , R_y and R_z directions respectively; (b) The corresponding absolute registration error in degrees.

5. Conclusion

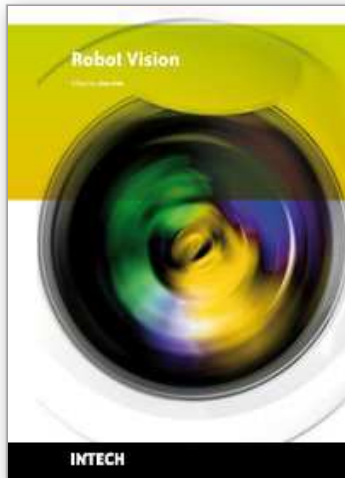
The results indicate that the pose estimation framework discussed in this chapter is able to identify the orientation of femur shaft fracture segments in 3D with acceptable accuracies, from 2D orthogonal views. The registration was performed at sub-degree accuracy with successful repeatability. Future testing will be conducted by the authors with the aid of actual intra-operatively obtained fluoroscopic images. The authors are also exploring techniques to further augment the pose estimation performed through the 2D-3D registration. One such measure includes skin based markers that may be employed to identify the axial misalignment between the proximal and distal segments. This axial alignment has been identified as one of the vital requirements for clinically successful fracture reduction surgery.

6. References

- Besl, P. J. and N. D. McKay. (1992). "A method for registration of 3-D shapes." *IEEE Transactions on pattern analysis and machine intelligence* **14**(2): 239-256.
- Beutel, J., H. L. Kundel, et al., Eds. (2000). *Handbook of Medical Imaging*. Bellingham, SPIE Press.
- Bollet, M. A., H. A. Mcnair, et al. (2003). "Can Digitally Reconstructed Radiographs (DRRS) Replace Simulation Films in Prostate Cancer Conformal Radiotherapy?" *Int. J. Radiation Oncology Biol. Phys* **57**(4): 1122-1130.
- Cure-Research. (2004). "http://www.cureresearch.com/f/fractured_femur/stats-country.htm." Fracture Statistics.
- Gamage, P., S. Q. Xie, et al. (2008). Intra-Operative 3D Pose Estimation of Fractured Bone Segments for Image Guided Orthopedic Surgery. *IEEE International Conference on Robotics and Biomimetics*. Bangkok, IEEE.
- Graham, A. E. and S. Q. Xie (2007). *Robotic Long Bone Fracture Reduction*. Medical Robotics. V. Bozovic, i-Tech Education and Publishing: 85-102.
- Hüfner, T., R. Meller, et al. (2005). "The role of navigation in knee surgery and evaluation of three-dimensional knee kinematics." *Oper. Tech. Orthop.* **15**: 64-69.
- Joskowicz L, Milgrom C, et al. (1998). "FRACAS: A System for Computer-Aided Image-Guided Long Bone Fracture Surgery." *Comp Aid Surg*: 271-288.
- Kim, Y. H., J. K. Kim, et al. (2004). "Three-dimensional reconstruction of human femur using consecutive computer tomography images and simulated implantation system." *Med. Eng. Technol* **28**: 205-210.
- Lagarias, J. C., J. A. Reeds, et al. (1998). "Convergence Properties of the Nelder-Mead Simplex Method in Low Dimensions." *SIAM Journal of Optimization* **9**(1): 112-147.
- LaRose, D., J. Bayouth, et al. (2000). Transgraph: Interactive intensity-based 2D/3D registration of X-ray and CT data. *Proceedings of SPIE - The International Society for Optical Engineering, Society of Photo-Optical Instrumentation Engineers*.
- LaRose, D., L. Cassenti, et al. (2000). Postoperative measurements of acetabular Cup Position Using X-Ray/CT registration. *MICCAI*.
- Lavallee, S., R. Szeliski, et al. (1995). *Anatomy-Based Registration of Three Dimensional Medical Images, Range Images, X-Ray Projections, and Three Dimensional Models Using Octree-Splines*. Computer-integrated surgery, technology and clinical applications. R. H. Taylor: 115-144.
- Li, C., C. Xu, et al. (2005). Level Set Evolution Without Re-initialization: A New Variational Formulation. *Proceedings of the 2005 IEEE Computer Society Conference on Computer Vision and Pattern Recognition (CVPR'05)*.
- Livyatan, H., Z. Yaniv, et al. (2003). "Gradient-Based 2-D/3-D Rigid Registration of Fluoroscopic X-Ray to CT." *IEEE Transactions on Medical Imaging* **22**(11): 1395-1406.
- Miyamoto, S., M. Sugiura, et al. (2003). "Development of Minimally Invasive Surgery Systems." *Hitachi Review* **52** (4): 189-195.
- Momi, E. D., B. Motyl, et al. (2005). Hip joint anatomy virtual and stereolithographic reconstruction for preoperative planning of total hip replacement. *Proceedings of CARS 2005 International Congress Series Elsevier*
- Noble, P. C., J. W. Alexander, et al. (1988). "The Anatomic Basis of Femoral Component Design." *Clinical Orthopaedics and Related Research* **235**: 148-165.

- Penney, G. P., P. G. Batchelor, et al. (2001). "Validation of a 2D to 3D registration algorithm for aligning preoperative CT images and intraoperative fluoroscopy images." *Med. Phys.* **28**(6).
- Penney, G. P., J. Weese, et al. (1998). "A Comparison of Similarity Measures for Use in 2D-3D Medical Image Registration." *IEEE Transactions on Medical Imaging* **17**(4): 586-595.
- Penny, G. P. (1999). *Registration of Tomographic Images to X-ray Projections for Use in Image Guided Interventions*. London, University of London. **PhD**.
- Rohlfing, T. and C. R. Maurer (2002). A novel image similarity measure for registration of 3-D MR images and X-ray projection images. *Medical Image Computing and Computer Assisted Intervention Conf.*
- Taylor, R. H., B. D. Mittelstadt, et al. (1994). "An image-directed robotic system for precise orthopedic surgery." *IEEE Trans. Robot. Automat.* **10**: 261-275.
- Tomaževic, D. (2002). *2D-3D Registration of Medical Images*. Faculty of Electrical Engineering. Ljubljana, University of Ljubljana.
- Tomaževic, D., B. Likar, et al. (2003). "3-D/2-D Registration of CT and MR to X-Ray Images." *IEEE Transactions on Medical Imaging* **22**: 1407 - 1416.
- Tsai, R. (1987). "A versatile camera calibration technique for high-accuracy 3D machine vision metrology using off-the-shelf TV cameras and lenses." *IEEE Journal in Robotics and Automation* **RA-3**(4): 323-344.
- Westphal R, Winkelbach S, et al. (2007). *Telemanipulated Long Bone Fracture Reduction*.
- Westphal, R., S. Winkelbach, et al. (2007). *Telemanipulated Long Bone Fracture Reduction*.
- Zollei, L. (2001). *2D-3D Rigid-Body Registration of X-Ray Fluoroscopy and CT Images*. Electrical Engineering and Computer Science. Massachusetts, Massachusetts Institute of Technology. **Masters**.
- Zollei, L., W. E. L. Grimson, et al. (2001). 2D-3D rigid registration of X-ray fluoroscopy and CT images using mutual information and sparsely sampled histogram estimators. *IEEE Computer Vision and Pattern Recognition Conf.*

IntechOpen



Robot Vision

Edited by Ales Ude

ISBN 978-953-307-077-3

Hard cover, 614 pages

Publisher InTech

Published online 01, March, 2010

Published in print edition March, 2010

The purpose of robot vision is to enable robots to perceive the external world in order to perform a large range of tasks such as navigation, visual servoing for object tracking and manipulation, object recognition and categorization, surveillance, and higher-level decision-making. Among different perceptual modalities, vision is arguably the most important one. It is therefore an essential building block of a cognitive robot. This book presents a snapshot of the wide variety of work in robot vision that is currently going on in different parts of the world.

How to reference

In order to correctly reference this scholarly work, feel free to copy and paste the following:

P. Gamage, S. Q. Xie, P. Delmas and W. L. Xu (2010). Vision Based Robotic Navigation: Application to Orthopedic Surgery, Robot Vision, Ales Ude (Ed.), ISBN: 978-953-307-077-3, InTech, Available from: <http://www.intechopen.com/books/robot-vision/vision-based-robotic-navigation-application-to-orthopedic-surgery>

INTECH
open science | open minds

InTech Europe

University Campus STeP Ri
Slavka Krautzeka 83/A
51000 Rijeka, Croatia
Phone: +385 (51) 770 447
Fax: +385 (51) 686 166
www.intechopen.com

InTech China

Unit 405, Office Block, Hotel Equatorial Shanghai
No.65, Yan An Road (West), Shanghai, 200040, China
中国上海市延安西路65号上海国际贵都大饭店办公楼405单元
Phone: +86-21-62489820
Fax: +86-21-62489821

© 2010 The Author(s). Licensee IntechOpen. This chapter is distributed under the terms of the [Creative Commons Attribution-NonCommercial-ShareAlike-3.0 License](#), which permits use, distribution and reproduction for non-commercial purposes, provided the original is properly cited and derivative works building on this content are distributed under the same license.

IntechOpen

IntechOpen